An Operational Approach for Generating the Global Land Surface Downward Shortwave Radiation Product From MODIS Data

Xiaotong Zhang, Dongdong Wang, Qiang Liu, Yunjun Yao, Kun Jia, Tao He, Bo Jiang, Yu Wei, Han Ma, Xiang Zhao, Wenhong Li, and Shunlin Liang, *Fellow, IEEE*

***Abstract*— Surface shortwave net radiation (SSNR) and surface downward shortwave radiation (DSR) are the two surface shortwave radiation components in earth's radiation budget and the fundamental quantities of energy available at the earth's surface. Although several global radiation products from global circulation models, global reanalyses, and satellite observations have been released, their coarse spatial resolutions and low accuracies limit their application. In this paper, the Global LAnd Surface Satellite (GLASS) DSR product was generated from the Moderate Resolution Imaging Spectroradiometer top-of-atmosphere (TOA) spectral reflectance based on a direct-estimation method. First, the TOA reflectances were derived based on the atmospheric radiative transfer simulations under different solar/view geometries; second, a linear regression relationship between the TOA reflectance and SSNR was developed under various atmospheric conditions and surface properties for different solar/view geometries; third, the coefficients derived from the linear regression were used to compute the SSNR; and finally, the DSR was estimated using the SSNR estimates and broadband albedo at the surface. A 13-year (2003–2015) GLASS DSR product was generated at a 5-km spatial resolution and 1-day temporal resolution. Compared with the ground measurements collected from 525 stations from 2003 to 2005 around the world, the model-computed SSNR (DSR) had an overall bias of 8.82 (3.72) W/m^2 and a root mean square error of 28.83 (32.84) W/m^2 at the daily time scale. Moreover, the global land annual mean of the DSR was determined to be 184.8 W/m^2 with a standard deviation of 0.8 W/m^2 over a 13-year (2003–2015) period.**

***Index Terms*— Globalirradiance, incident shortwave radiation, remote sensing.**

Manuscript received December 12, 2017; revised April 28, 2018 and November 29, 2018; accepted December 31, 2018. Date of publication February 1, 2019; date of current version June 24, 2019. This work was supported in part by the National Key Research and Development Program of China under Grant 2016YFA0600102, in part by the National Natural Science Foundation of China under Grant 41571340, and in part by the National Basic Research of China under Grant 2015CB953701. *(Corresponding author: Xiaotong Zhang.)*

X. Zhang, Y. Yao, K. Jia, B. Jiang, Y. Wei, and X. Zhao are with the State Key Laboratory of Remote Sensing Science, Jointly Sponsored by Beijing Normal University and Institute of Remote Sensing and Digital Earth of Chinese Academy of Sciences, Beijing 100875, China, and also with the Beijing Engineering Research Center for Global Land Remote Sensing Products, Faculty of Geographical Science, Institute of Remote Sensing Science and Engineering, Beijing Normal University, Beijing 100875, China (e-mail: xtngzhang@bnu.edu.cn).

D. Wang is with the Department of Geographical Sciences, University of Maryland at College Park, College Park, MD 20742 USA (e-mail: ddwang@umd.edu).

Q. Liu is with the State Key Laboratory of Remote Sensing Science, Institute of Remote Sensing and Digital Earth, Jointly Sponsored by Beijing Normal University and Institute of Remote Sensing and Digital Earth of Chinese Academy of Sciences, Beijing 100875, China, and also with the College of Global Change and Earth System Science, Beijing Normal University, Beijing 100875, China (e-mail: toliuqiang@bnu.edu.cn).

T. He and H. Ma are with the School of Remote Sensing and Information Engineering, Wuhan University, Wuhan 43079, China (e-mail: taohers@whu.edu.cn).

W. Li is with the Nicholas School of the Environment, Duke University, Durham, NC 27708 USA (e-mail: wenhong.li@duke.edu).

S. Liang is with the Department of Geographical Sciences, University of Maryland at College Park, College Park, MD 20742 USA, and also with the School of Remote Sensing and Information Engineering, Wuhan University, Wuhan 43079, China.

Color versions of one or more of the figures in this paper are available online at http://ieeexplore.ieee.org.

Digital Object Identifier 10.1109/TGRS.2019.2891945

I. Introduction

KNOWLEDGE of the earth's radiation budget is essential for improving our understanding of earth's climate and the processes and interactions taking place within it [1]–[5]. Surface shortwave net radiation (SSNR), also known as surface absorbed shortwave radiation, and surface downward shortwave radiation (DSR) are the two surface shortwave radiation components in the earth's radiation budget. SSNR and DSR are also the two fundamental quantities of energy available at the earth's surface, which affect temperature fields, atmospheric and oceanic circulations, and hydrological cycles [6]–[8]. Remote sensing, which provides unparalleled spatial and temporal coverage of land surface attributes, has contributed to the improved estimation of the earth's radiation budget during last several decades. However, a comparison between four current representative satellite DSR products and direct surface measurements showed that large uncertainties are still present in the current satellite-derived DSR products and that their coarse spatial resolutions and low accuracies limit their applications in the land communities [5].

Many studies have attempted to estimate the DSR [9]–[24] and SSNR [3], [6]–[8], [25]–[28] using satellite observations and ancillary information. Based on these studies, numerous methods have been developed to retrieve SSNR and DSR from satellite signals. The SSNR is usually estimated as the product of the DSR and surface albedo. The uncertainties existing in DSR [5], [29]–[32] and surface broadband shortwave albedo [33]–[35] may cause large errors in SSNR estimation. An alternative method is to estimate the SSNR directly from the top-of-atmosphere (TOA) signature received by the satellite sensors [3], [7], [8], [27], [28]. Li *et al.* [3], [27]

reported that SSNR could be related to the normalized outgoing flux at the TOA. Tang *et al.* [28] adopted the parameterization schemes from Li *et al.* [3], [27] and provided variable coefficients under different land cover types to estimate the SSNR using the Moderate Resolution Imaging Spectroradiometer (MODIS) observations by converting the narrowband MODIS TOA reflectance into a TOA broadband albedo. Direct-estimation methods that estimate the SSNR from spectral TOA reflectance from hyperspectral Airborne Visible/Infrared Imaging Spectrometer and MODIS data were also developed by He *et al.* [6] and Kim and Liang [7], respectively.

Currently, the DSR can be calculated from satellite observations by three common approaches. First is to develop regressions based on simultaneous and collocated satellite TOA radiance and radiative fluxes observed at the surface [36], [37]. The second is to develop retrieval schemes to calculate the DSR in terms of scattering, reflection, and absorption variables in radiative transfer models or parameterized models to deduce atmospheric transmittances using atmospheric, cloud, and land surface variables as the input data [1], [9], [13]–[15], [18], [38]–[43]. The third is to estimate the DSR by matching radiative transfer computations and satellite observations based on a lookup table that is constructed through complex radiative transfer simulations [11], [12], [18], [19].

Based on the aforementioned methods, several global SSNR and DSR satellite radiation products have been generated, such as the Global Energy and Water Cycle Experiment—Surface Radiation Budget (GEWEX-SRB) and the Earth's Radiant Energy System (CERES) EBAF. However, their spatial resolutions are always limited and cannot match, very well, the requirements of practical applications, such as hydrological and ecological modeling. Moreover, large uncertainties still exist in current global satellite products. As pointed out by Zhang *et al.* [5], four current representative satellite products overestimate the DSR by approximately 10 W/m^2 at the monthly time scale. Large discrepancies were also found in current global satellite DSR products over the highly variable terrain of the Tibet Plateau by Gui *et al.* [29] and Yang *et al.* [44]. In addition, most of these products have been validated using the limited surface observations, especially for the SSNR. Therefore, it is still necessary to develop new methods to generate high spatial resolution radiation products and evaluate them as many surface measurements as possible.

This paper attempts to generate a global daily DSR product at a 5-km spatial resolution and 1-day temporal resolution from MODIS data using a revised direct-estimation method. The generated products are validated using the ground measurements collected from the Baseline Surface Radiation Network (BSRN), the Global Energy Balance Archive (GEBA), and the Climate Data Center of the China Meteorological Administration (CDC/CMA) from 2003 to 2005. Moreover, the DSR estimates are also aggregated for comparison with the corresponding GEWEX-SRB, CERES-EBAF, and ERA-Interim data. This paper is organized as follows. Section II introduces the satellite and ground measurement data used, Section III describes the methods used, Section IV shows the results and analysis, and a short summary and the conclusions are provided in Section V.

II. Data

A. Ground Measurements

Ground measurements of the downward and upward shortwave radiation from BSRN, GEBA, and CDC/CMA data sets are publicly available. Compared to the DSR surface measurements from these three databases, upward shortwave radiation measurements were originally provided at only four stations from BSRN and 17 stations from CDC/CMA. In this paper, the ground measurements obtained from these three databases were used to evaluate the SSNR and DSR derived from the MODIS observations.

To date, the BSRN project has archived ground measurements at more than 60 sites, covering a wide latitudinal range from $-89.98°$ to $82.49°$ and a longitudinal range from $-156.61°$ to $169.69°$, where the earliest BSRN records start in January, 1992. BSRN was established to provide high-quality validation data sources for satellite retrievals and climate models and are recognized as the most reliable data network available today. To use the BSRN data to validate the retrieved SSNR and DSR, the former must be processed to generate daily and monthly means because the estimated SSNR and DSR are available on these two time scales. The DSR was directly measured at the BSRN sites, whereas the SSNR was calculated as the difference between downward and upward solar radiation. GEBA is a fundamental database of worldwide and instrumentally measured surface energy fluxes, developed and maintained at the ETH Zürich [45]. GEBA provides data from 2500 stations, with 450 000 monthly mean values of various surface energy balance components. Monthly mean DSRs were collected at 395 stations via GEBA. The CDC/CMA releases daily and monthly meteorological measurement data at 122 routine weather stations. In this paper, a set of quality check procedures was also conducted for DSR before any comparisons were made. The quality of the ground measured DSR data was controlled based on the surface-reconstructed DSR data using routine meteorological data, including air temperature, air pressure, relative humidity, sunshine duration, and precipitation [5], [19]. Quality control of the upward solar radiation data was performed before the release by CDC/CMA, including a spatial and temporal consistency check, and manual inspection and correction. Table I lists detailed information on the ground measurements used in this paper.

The evaluation in this paper was conducted for the time period of 2003–2005. A total of 525 stations were used to validate the DSR retrievals, including 36 stations from BSRN, 395 stations from GEBA, and 94 stations from CMA. Among these sites, 22 stations (five stations from BSRN and 17 stations from CDC/CMA) that provided the SSNR observations were used to validate the SSNR retrievals from the MODIS observations. Fig. 1 shows the geographical distributions of the observation sites used in this paper.

TABLE I
DETAILS OF THE DATA PRODUCTS USED IN THIS COMPARISON

Data Source	Data period	Temporal resolution	Spatial resolution
GEBA	1922-2008	monthly	N/A(station)
BSRN	1992-present	1 minute	N/A(station)
CMA	1957-present	daily	N/A(station)
CERES-EBAF	2000-present	monthly	1°×1°
ERA-Interim	1979-present	3h	0.75°×0.75°
GEWEX-SRB	1983-2007	daily	1°×1°
This study	2000-2015	daily	5km×5km

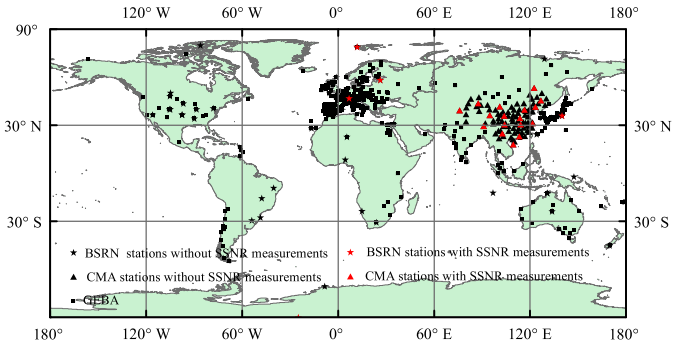

Fig. 1. Geographical distribution of observation sites (525 sites in total) used in this paper from GEBA (395 sites in squares), BSRN (36 sites in asterisks), and CMA (94 sites in triangles). Red color indicates that these stations not only provide DSR measurements but also SSNR measurements.

B. MODIS Data

TOA reflectance data (MOD021KM and MYD021KM) and the related geolocation data (MOD03 and MYD03) were obtained from the MODIS level 1B data set (C06). The MOD021KM and MYD021KM data are the calibrated earth view data at 1-km resolution, including the 250- and 500-m resolution bands aggregated to 1-km resolution [46]. The first seven spectral bands (bands 1–7) and band 19 of the MOD021KM and MYD021KM data sets are used in this paper. The MOD03 and MYD03 products provide geolocation fields data calculated for each 1-km MODIS instantaneous field of view [47]. Cloud mask data (MOD35 and MYD35) from both the Terra and Aqua satellites are also used for SSNR and DSR retrievals [48]. In this paper, both the Terra and Aqua data are also used to generate the DSR product because it has been proven that SSNR estimates achieve a higher correlation with ground measurements when the observations from both the Terra and Aqua satellites are combined than when the estimates are based on data from a single MODIS sensor.

C. GLASS Albedo

Land surface albedo is an essential parameter in surface radiation budget studies. Although global and regional broadband surface albedo products have been generated using satellite observations, many of land surfaces are underrepresented. For example, albedo over snow- and ice-covered surfaces is usually missed. The daily mean Global LAnd Surface Satellite (GLASS) broadband albedo product, which is spatial and temporal continuous, is used to calculate the DSR at earth's surface in this paper. The GLASS broadband albedo was estimated using MODIS data based on a direct-estimation algorithm [33], [49] with the main objective of establishing a relationship between the broadband albedo and TOA reflectance. The coefficients for converting TOA reflectance into broadband surface albedo for different solar/view geometries were calculated beforehand and stored in the lookup tables. The coefficients were derived based on the following steps: 1) establishing the bidirectional reflectance distribution function (BRDF) database using the Polarization and Directionality of the earth's Reflectances/Polarization and Anisotropy of Reflectances for Atmospheric Sciences coupled with Observations from a LiDAR BRDF database; 2) converting the narrowband into broadband albedo based on the surface BRDF database; 3) deriving the TOA reflectance based on the atmospheric radiative transfer simulations; and 4) determining the relationship between TOA reflectance and surface broadband albedo for each solar/viewing angular bin. The spatial and temporal resolutions of the GLASS broadband shortwave albedo are 5 km and 1 day, respectively.

D. Existing Radiation Products

1) CERES-EBAF: The CERES-EBAF DSRs were computed using the cloud and aerosol properties derived from instruments on the A-train constellation using a radiative transfer model with a k-distribution and correlated-k for radiation with a two-stream approximation [41]. The CERES-EBAF was estimated based on the following main steps.

1) Determine the 1° monthly mean differences between the computed TOA fluxes from SYN1deg-Month and the fluxes from CERES EBAF-TOA.
2) Correct the DSR errors due to the error in the space view cloud fraction.
3) Use a Lagrange multiplier procedure to determine the perturbations in surface, cloud, and atmospheric properties to match the TOA flux differences.
4) Compute the change in surface flux based on these perturbed surface, cloud, and atmospheric properties.

The CERES-EBAF v2.8 DSR data set is a gap-filled product with a monthly temporal resolution and a 1° spatial resolution from March, 2000 to February, 2017.

2) GEWEX-SRB: The other satellite-derived DSRs used in this paper were obtained from the NASA/GEWEX-SRB v3.0 data set. The core of the GEWEX-SRB algorithm is an updated version of the University of Maryland Algorithm [14]. The GEWEX-SRB v3.0 data set estimates the DSRs at the earth's surface on the basis of cloud fraction, atmospheric composition, background aerosols, and spectral albedo with TOA-measured cloudy and clear-sky radiances acting as constraints through radiative transfer computations. The GEWEX-SRB DSR data were provided with temporal resolutions of 3 hours, daily, and monthly and a spatial resolution of 1° from July, 1983 to December, 2007.

3) ERA-Interim: ERA-Interim is a global atmospheric reanalysis product generated by the ECMWF, which has the data available since 1979 [50], [51]. The ERA-Interim project was initiated in part to prepare for a new atmospheric reanalysis to replace ERA-40. The spatial resolution of the

TABLE II
VIEW GEOMETRY, WATER-VAPOR CONCENTRATIONS, AEROSOLS, AND CLOUDS PROPERTIES USED IN THE ATMOSPHERIC RADIATIVE TRANSFER SIMULATIONS

Data Source	Clear-sky Conditions	Cloudy-sky conditions
Solar Zenith Angle	0° 10° 20° 30° 45° 60° 75°	
View zenith angle	0° 10° 20° 30° 45° 60°	
Relative azimuth angle	0° 30° 60° 90° 120° 150° 180°	
Water vapor(g/cm2)	0.5, 1.0, 1.5, 3.0, 5.0, 7.0	1.5, 3.0, 7.0, 12.0
Aerosols	rural, urban, desert, and Tropospheric (0.0 0.1 0.2 0.3 0.4)	Rural (0.1)
Clouds		stratus, cumulus, altostratus, and nimbostratus

ERA-Interim data set is 0.75° (approximately 80 km) over 60 vertical levels from the surface up to 0.1 hPa. Radiation is calculated based on the Rapid Radiation Transfer Model [52]. The ERA-Interim DSR data were provided at a temporal resolution of 3 h and a spatial resolution of 0.75° from 1979 to present.

III. DSR RETRIEVAL SCHEMES

A. Retrieval Algorithm

SSNR was estimated from MODIS TOA spectral data based on a direct-estimation method proposed by Wang *et al.* [8]. Daily SSNR ($S_{\text{net}}^{\text{daily}}$) can be estimated from MODIS TOA spectral radiance data under a given viewing geometry, which is defined as a combination of the solar zenith angle (θ), viewing zenith angle (ϕ), and relative azimuth angle (φ), using the following equation:

$$S_{\text{net}}^{\text{daily}} = c_0(\Omega, \zeta) + \sum_b c_b(\Omega, \zeta) \bullet r_b \tag{1}$$

where c_0 represents the offset and c_b represents the coefficient for band b from MODIS [bands 1–7 (land bands) and band 19 (water-vapor absorption band)]. The regression coefficients are obtained from an extensive atmospheric radiative transfer simulation using MODTRAN under representative surface and atmospheric conditions for a given viewing geometry (Ω). The regression coefficients (c_0 and c_b) are also dependent on the cloud condition (ζ, clear or cloudy sky).

A library of 245 surface spectra database was used as the surface boundary conditions for radiative transfer simulation using MODTRAN. In terms of atmospheric parameters, the clear-sky simulations mainly considered variations in aerosols and the water-vapor concentration, whereas the cloud optical depth (COD) and the water-vapor concentration were mainly considered in the atmospheric radiative simulations. Four aerosol types (rural, urban, desert, and tropospheric) and four types of clouds were considered for the clear-sky and cloudy-sky simulations. Table II summarizes the viewing geometries, water-vapor concentrations, aerosols, and cloud properties used in the atmospheric radiative transfer simulations. MODTRAN can directly produce instantaneous SSNR values. Daily SSNR values can be estimated by integrating instantaneous values, as in the following equations:

$$S_{\text{net}}^{\text{daily}} = \frac{\int S_{\text{net}}^{\text{ins}}(t)dt}{T} \tag{2}$$

where T represents the length of one day (24 h).

For a given daily SSNR ($S_{\text{net}}^{\text{daily}}$) and daily surface albedo, the daily DSR (S^{daily}) can be estimated based on the following equation:

$$S^{\text{daily}} = S_{\text{net}}^{\text{daily}}/(1-\alpha) \tag{3}$$

where α represents the GLASS albedo product.

The monthly SSNR and DSR were obtained from the retrieved daily SSNR and DSR data by summing the daily SSNR and DSR, respectively. If daily SSNR and DSR data were missing for less than nine days, the monthly SSNR and DSR were estimated using the following equation:

$$S^{\text{month}} = \left(\sum_{i=1}^{n} S^{\text{daily}}/n\right) * N \tag{4}$$

where n represents the number of the estimated daily SSNR or DSR is values available in one month, N represents the total number of days in one month, S^{daily} represents the daily estimated SSNR or DSR, and S^{month} represents the monthly estimated SSNR or DSR.

B. Generating Global Land DSR Products

Although many efforts have been reported to develop a DSR retrieval algorithm, only several global DSR products have been generated based on the proposed method. Therefore, much work needs to be done to generate a global product, especially at a higher spatial resolution. The MODIS TOA geolocation (MOD03 and MYD03), TOA reflectance (MOD02 and MYD02), and cloud mask (MOD35 and MYD35) products are the calibrated earth view data at a 1-km resolution. First, we estimated the SSNR based on the proposed direct-estimation method at a 1-km spatial resolution onboard both the Terra and Aqua satellites. Second, the estimated SSNRs were projected onto a 5-km spatial resolution for MODIS data from both the Terra and Aqua satellites. A minimum of one value of the daily SSNR can be obtained for each MODIS observation. The local overpass times for the MODIS Terra and Aqua is around 10:30 A.M. and 1:30 P.M., respectively. It is important to integrate the daily mean SSNR to have both morning and afternoon observation because the atmospheric conditions often show distinct patterns in the morning and afternoon. The MODIS observation frequency is dependent on latitude, and higher latitudes observe more MODIS overpasses. If more than one observations were available for a single day, we averaged the estimates for that day to obtain the final mean daily value. After combining the MODIS observations from both the Terra and Aqua satellites, daily estimates exhibited a higher correlation with the ground measurements and a reduced root mean square error (RMSE) of 6–7 W/m^2, compared with the SSNR estimates based on data from an individual MODIS sensor (Terra or Aqua) [8]. Third, the global land surface DSRs were derived using the SSNR estimates and GLASS broadband albedo. Even though

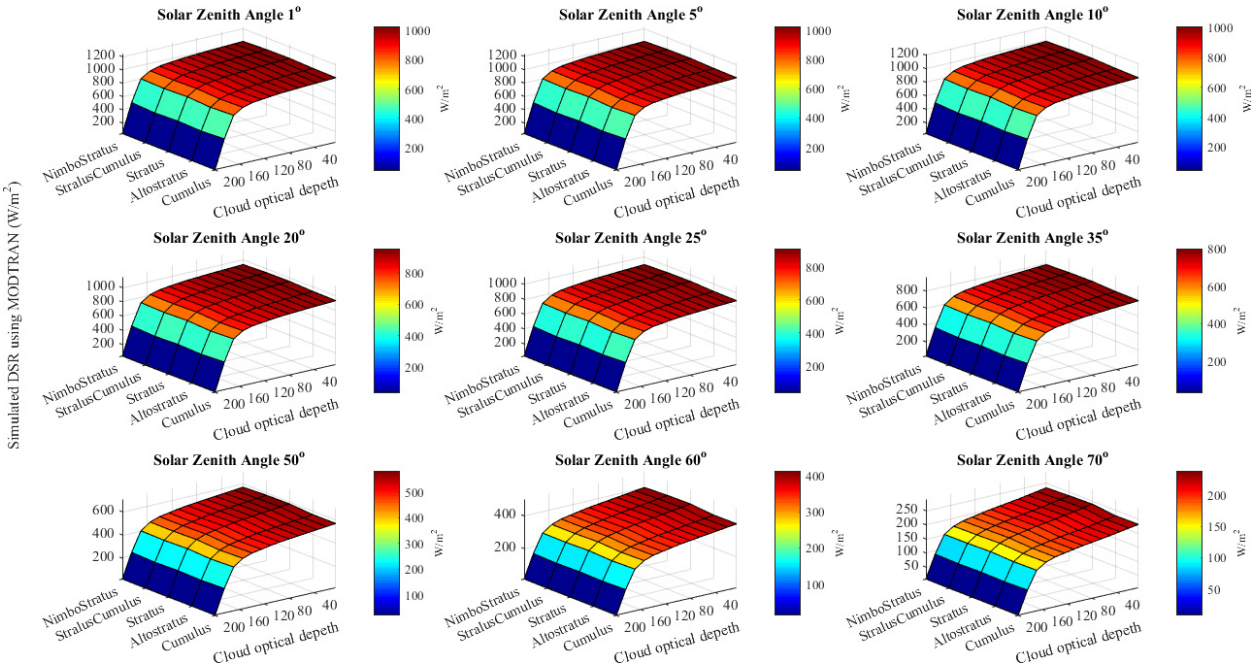

Fig. 2. Sensitivity of DSR to cloud types with changing COD (varies from 0.1 to 200) under different solar zenith angles. The atmospheric condition is represented by a mid-latitude summer atmosphere (water vapor: 1.0 gm/m2; visibility: 10 km; and albedo: 0.10).

the MODIS observations from both the Terra and Aqua satellites were used, certain gaps still existed over low-latitude areas. Finally, the spatially continuous daily mean DSRs were estimated by the nearest neighbor interpolation method.

C. Sensitivity Analysis

Previous studies have pointed out that clouds and aerosols are the main factors affecting the planetary energy balance and, therefore, modulating climate. More specifically, aerosols may affect climate through their direct effect (i.e., attenuating surface solar radiation by scattering and absorbing) [53] on radiation and indirect effects associated with interactions with clouds (i.e., increasing cloud reflectivity and lifetime via their ability to act as cloud condensation nuclei) [54]. Therefore, the sensitivity analysis was tested to determine the dependence of the DSR on cloud and aerosol types in this paper. Fig. 2 shows the sensitivity experimental results of DSR to different cloud types (Nimbostratus, Stratocumulus, Stratus, Altostratus, and Cumulus) with changing COD (varies from 0.1 to 200) under different solar zenith angles. The atmospheric condition is represented by a mid-latitude summer atmosphere (water vapor: 1.0 gm/m^2; visibility: 23 km; and albedo: 0.10). As shown in Fig. 2, differences of the simulated DSR were relatively small for these five selected cloud types with changing COD under different solar zenith angles. This result suggests that the cloud types have relatively minor impacts on DSR estimation. To evaluate the effects of aerosol models on the DSR simulations using MODTRAN, we carried out experiments to test the sensitivity of DSR to different aerosol modes with changing meteorological visibility range (varies from 10 to 100 km) under different solar zenith angles (see Fig. 3). Five basic aerosol modes (rural, urban, desert, tropospheric, and maritime) were selected to represent atmospheric turbidity in MODTRAN, and the atmospheric condition was represented by a mid-latitude summer atmosphere (water vapor: 1.0 gm/m^2; albedo: 0.10: and wind speed for desert aerosol mode: 10 m/s). Fig. 3 shows that the impacts of aerosol types on DSR estimation are significant, especially for the lower meteorological visibility range. For example, the maximum absolute difference of DSR estimation between the rural and tropospheric aerosol model was greater than 100 W/m^2 at 10-km visibility under 1° solar zenith angle. It is also shown that the impacts of aerosol type on DSR estimation decreased with an increasing meteorological visibility range. Thus, we used multiple aerosol and cloud types to obtain the representative coefficients to calculate the SSNR and DSR in this paper.

IV. Results and Analysis

A. Validation of SSNR Estimates

For ground measurements, the SSNR was calculated as the difference between DSR and upward solar radiation. High-quality ground-measured SSNR data were taken from two sources: the CDC/CMA and the BSRN. As presented previously, only five stations from the BSRN and 17 stations from the CDC/CMA provided upward shortwave radiation ground measurements for the time period 2003–2005; therefore, the daily and monthly SSNRs were validated at the selected 22 stations.

1) Evaluation at a Daily Time Scale: Fig. 4(a) shows a scatterplot representing a comparison of the ground measurements versus the estimated daily mean SSNR for all 22 BSRN stations within the $1° \times 1°$ cell containing each station. Table III lists the summarized results of the model-BSRN comparison in terms of bias, RMSEs, and correlation coefficient (R)

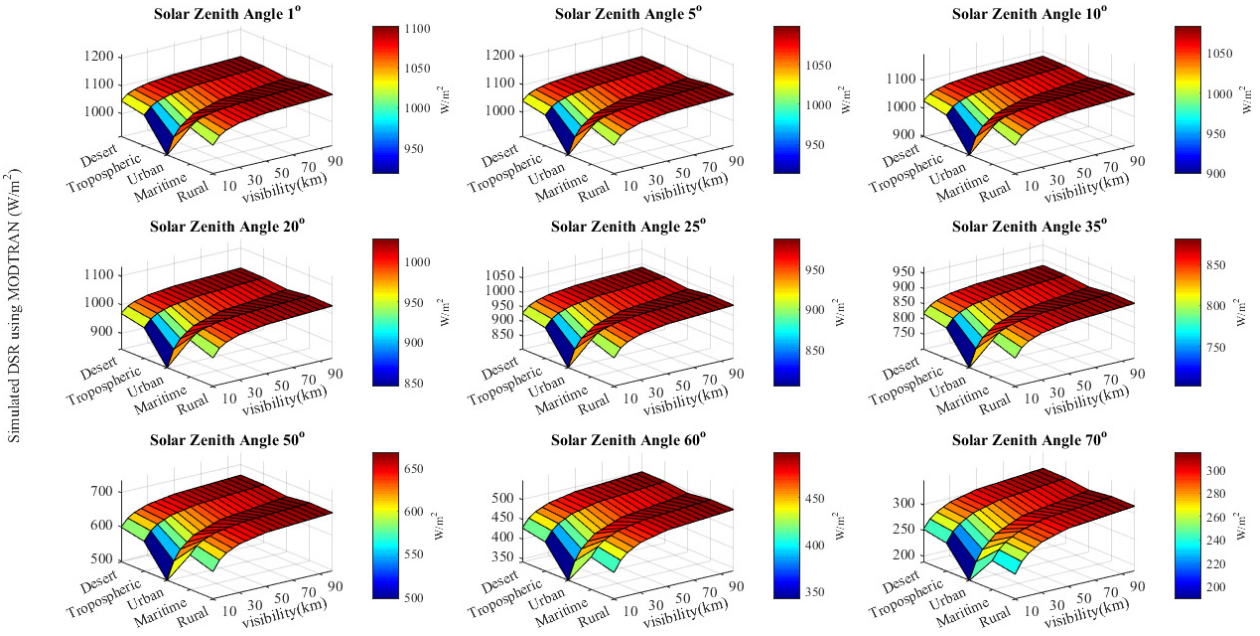

Fig. 3. Geographical distribution of observation sites (525 sites in total) used in this paper from GEBA (395 sites in squares), BSRN (36 sites in asterisks), and CMA (94 sites in triangles). Red color indicates that these stations not only provide DSR measurements but also SSNR measurements.

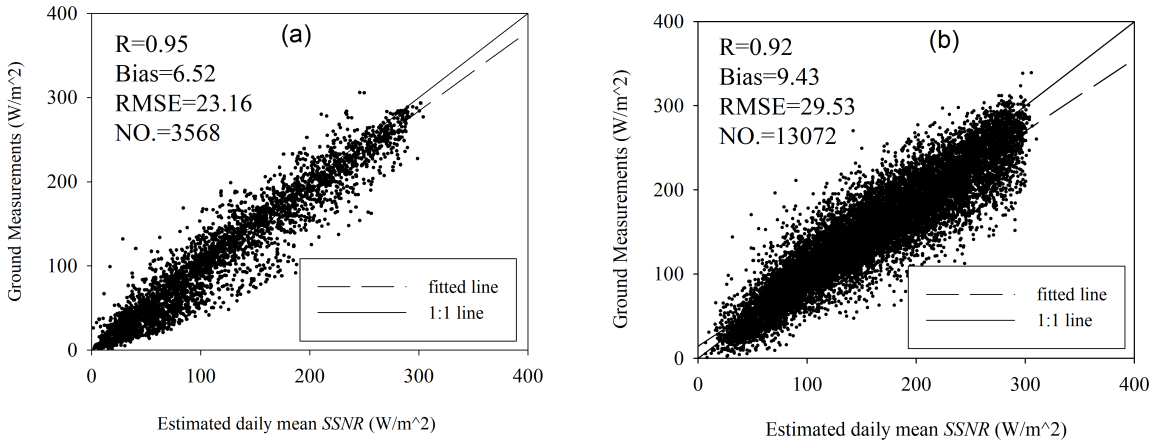

Fig. 4. Scatter plot comparison between model-computed and (a) BSRN and (b) CDC/CMA grid-cell data of daily average SSNR at the earth's surface, over the time period 2003–2005, respectively. *R* and *N* are the correlation coefficient and the number of matched data pairs, respectively.

for each station. The scatterplot shows a positive bias equal to 6.5 W/m^2 with a relatively small scatter. Further detailed analysis of the results evaluated against the ground measurements from the BSRN showed that the biases did not exceed 6 W/m^2, except at the Ny-Ålesund station (NYA) and South Pole station (SPO) stations. These two stations are located in a high-latitude area, whereas the other three stations are located in a mid-latitude area in the Northern Hemisphere. The largest biases were found at the NYA and SPO stations with the bias values of 11.0 and 27.9 W/m^2 and the RMSE values of 33.3 and 29.8 W/m^2, respectively. The model-computed discrepancies at high-latitude stations may be related to the polar climate because cloud detection is problematic over highly reflecting surfaces, such as those near the poles. Moreover, the precision of the radiative transfer model might be another potential error source over high-latitude areas. As noted by Zhang *et al.* [19] and Loeb and Davies [55], the accuracy of the radiative transfer simulation for larger solar zenith angles ($>63°$) is always limited, especially for plane-parallel model computations. A similar comparison of ground-measured against the model-computed daily mean SSNR fluxes was performed using another SSNR database (CDC/CMA). Similar to the validation results at the BSRN stations, the model-estimated SSNR shows a slight overestimation at the CDC/CMA stations, as shown in Fig. 4(b). A detailed analysis showed that the absolute error was less than 15 W/m^2 at ten out of 17 stations, and the RMSE was less than 30 W/m^2 at 11 out of 17 stations at a daily time scale (see Table III).

2) Evaluation at a Monthly Time Scale: Evaluations at a monthly time scale were also conducted at the BSRN and CDC/CMA stations (see Table III and Fig. 5). The

TABLE III

BSRN AND CDC/CMA STATIONS WITH MEASUREMENTS OF SSNR AT SURFACE IN THE PERIOD 2003–2005 USED FOR VALIDATION OF MODEL SSNR RESULTS AT DAILY AND MONTHLY TIME SCALES. LAT IS LATITUDE; LON IS LONGITUDE; BIAS IS THE AVERAGE DIFFERENCE OF ESTIMATED AND GROUND MEASURED FLUXES; RMSE IS THE ROOT MEAN SQUARE ERRORS; AND R IS THE CORRELATION COEFFICIENT

network	site code	Lat	Lon	daily			monthly		
				R	Bias	RMSE	R	Bias	RMSE
CDC /CMA	50136	53.47	122.52	0.92	-2.57	30.94	0.98	3.09	14.42
	50953	45.75	126.77	0.95	11.58	25.2	0.99	11.58	15.57
	51463	43.78	87.65	0.97	12.13	24.39	0.99	12.96	16.16
	51709	39.47	75.98	0.94	19.38	34.35	0.98	17.34	23.97
	52267	41.95	101.07	0.97	-2.81	20.08	0.99	-2.43	12.51
	52818	36.42	94.90	0.96	-12.29	22.53	0.99	-11.85	13.73
	52889	36.05	103.88	0.95	13.08	26.19	0.99	13.59	14.68
	54342	41.73	123.45	0.94	15.22	28.77	0.96	15.8	22.37
	54511	39.80	116.47	0.94	11.69	27.77	0.98	14	19.55
	55591	29.67	91.13	0.86	-11.28	29.82	0.95	-10.59	16.53
	56294	30.67	104.02	0.93	29.14	38.68	0.97	26.95	28.28
	56778	25.02	102.68	0.86	3.67	29.05	0.94	4.62	11.71
	57083	34.72	113.65	0.94	8.37	24.59	0.98	9.91	13.32
	57494	30.62	114.13	0.94	20.28	31.06	0.98	21.08	23.28
	58362	31.40	121.48	0.93	26.08	37.05	0.98	24.83	27.96
	59287	23.17	113.33	0.88	29.2	38.14	0.98	28.74	29.78
	59948	18.23	109.52	0.87	24.14	35.55	0.94	24.7	26.68
BSRN	NYA	78.93	11.93	0.87	11.02	33.34	0.89	10.73	22.82
	PAY	46.82	6.94	0.98	3.62	17.85	1.0	3.6	5.91
	SPO	-89.98	-24.80	0.76	27.93	29.79	0.92	28.66	29.37
	TAT	36.06	140.13	0.95	3.44	21.03	0.99	-7.47	9.87
	TOR	58.25	26.46	0.96	5.32	22.06	0.99	5.43	8.06
Mean	---	---	---	0.93	8.82	28.22	0.96	9.87	19.04

model estimated SSNR correlated very well with the ground measurements at both the BSRN and CDC/CMA stations with an overall R of 0.98, a positive bias of 3.6 W/m^2, and an RMSE of 13.6 W/m^2 at the BSRN stations, while these values were 0.95, 11.22 W/m^2, and 20.11 W/m^2 at the CDC/CMA stations, respectively. Similar to the evaluation results at the BSRN stations at a daily time scale, the largest biases were found at the stations in high-latitude areas. The RMSE values were less than 10 W/m^2 at the three stations located in the mid-latitude area. The R value was greater than 0.95 at 15 out of 17 stations, the absolute error was less than 15 W/m^2 at 11 out of 17 stations, and the RMSE was less than 30 W/m^2 at all 17 stations at a monthly time scale using the CDC/CMA database.

B. Validation of the GLASS DSR Product and Comparisons With Other Products

For the model-computed DSR estimates, not only were the model-estimated DSR fluxes evaluated against the ground measurements but also the evaluation results were compared with those estimated from the satellite-derived DSR from GEWEX-SRB at a daily time scale, the satellite-derived DSR from GEWEX-SRB and CERES-EBAF, and the predicted results of the reanalysis data from the ERA-Interim at a monthly time scale. The DSR data from these databases had different spatial resolutions (see Table I). The model-estimated DSR and the ERA-Interim DSR data were projected at a 1° spatial resolution to match that of the GEWEX-SRB and CERES-EBAF.

1) Evaluation and Comparison at a Daily Time Scale: Since the satellite-derived DSR data were only provided by GEWEX-SRB at a daily time scale, the DSR evaluations were performed for the model estimated and GEWEX-SRB v3.0 DSR products against the ground measurements from the BSRN and CDC/CMA stations at a daily time scale. Fig. 6(a) shows a scatterplot representing a comparison of the ground measurements versus the model-estimated daily mean DSR within $1° \times 1°$ cell containing each BSRN station. The scatterplot shows that the model estimated daily mean DSR correlated well with the ground measurements at the BSRN stations. The model-estimated DSR had an overall R value of 0.95, a negative bias of -3.30 W/m^2, and an RMSE of 30.93 W/m^2 at the BSRN stations with the valid ground measurements. A detailed analysis showed that the R values were greater than 0.95 at 20 out of 36 stations, the absolute error was less than 10 W/m^2 at 23 out of 36 stations, and the RMSE was less than 30 W/m^2 at 21 out of the 36 stations at the daily time scale for the BSRN database. To more thoroughly

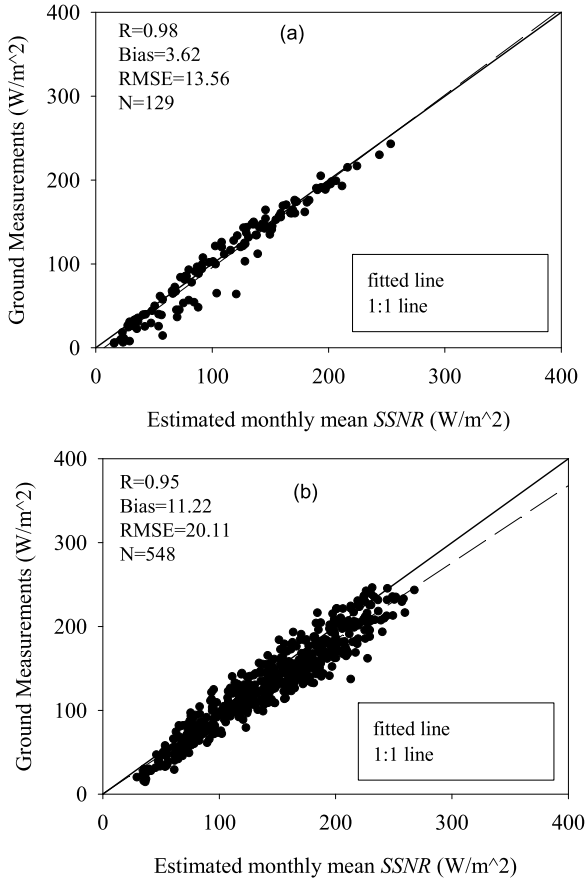

Fig. 5. Scatter plot comparison between model-computed and (a) BSRN and (b) CDC/CMA grid-cell data of monthly average SSNR at the earth's surface, over the time period 2003–2005, respectively. *R* and *N* are the correlation coefficient and the number of matched data pairs, respectively.

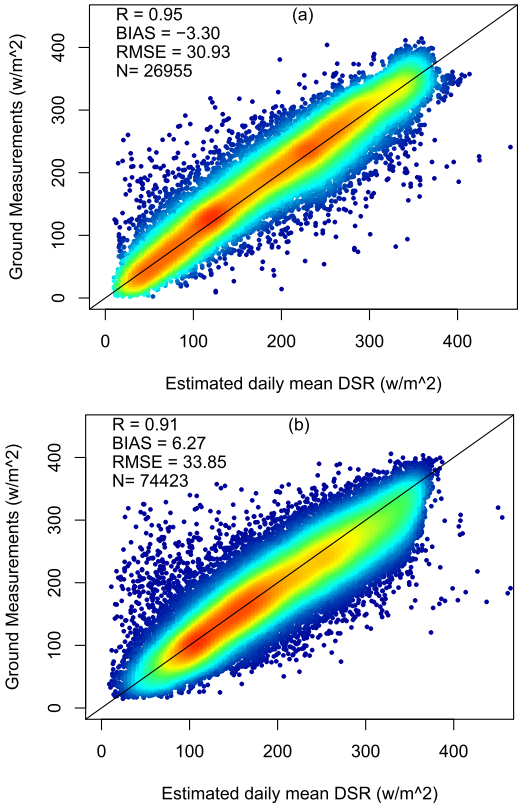

Fig. 6. Scatter plot comparison between the model-computed and the ground measurements of daily average DSR at (a) 36 stations from BSRN and (b) 94 stations from the CDC/CMA at the earth's surface, over the time period 2003–2005, respectively. *R* and *N* are the correlation coefficient and the number of matched data pairs, respectively.

assess the effect of the choice of surface observation stations and measurement quality on the model bias for the DSR, an ongoing analysis was repeated with a set of 94 CDC/CMA stations [see Fig. 6(b)]. As shown in Fig. 6(b), the model-estimated DSR exhibited a slight overestimation at the CDC/CMA stations with an *R* value of 0.91, a positive bias of 6.27 W/m^2, and an RMSE of 33.85 W/m^2. The absolute error was less than 10 W/m^2 at 28 out of 94 stations, and the RMSE was less than 30 W/m^2 at 36 out of the 94 stations at the daily time scale for the CDC/CMA database.

We also compared the validation results with those computed by existing DSR products. Among the three selected existing products, GEWEX-SRB was the only one that directly provided the daily DSR. The comparison results for the ground measurements versus the estimated daily mean DSR values within the $1^\circ \times 1^\circ$ cell containing each of the 36 BSRN and 94 CDC/CMA stations are shown in the scatterplots of Fig. 7(a) (BSRN) and (b) (CDC/CMA). The GEWEX-SRB had an *R* value of 0.92, a negative bias of -1.39 W/m^2, and an RMSE of 38.78 W/m^2 for the BSRN stations, whereas these values were 0.87, 0.11 W/m^2, and 38.14 W/m^2 for the CDC/CMA stations, respectively. It is obvious that both the model-computed and the GEWEX-SRB DSR products correlated well with ground measurements. Although the bias of the GEWEX-SRB DSR at both the BSRN and CDC/CMA stations was lower than that calculated from the model-computed DSR, the RMSEs of the GEWEX-SRB DSRs were greater than those derived from the model computed DSRs. This indicates that the GEWEX-SRB DSR is more scattered than the model-computed estimates, at least at the selected stations. A detailed analysis showed that the RMSE was less than 30 W/m^2 at ten out of 36 BSRN stations and three out of 94 CDC/CMA stations for the GEWEX-SRB DSR product, while the RMSE was less than 30 W/m^2 at 21 out of 36 BSRN stations and 36 out of 94 CDC/CMA stations for the model-computed DSR. According to the validation results at a daily time scale, the model-computed DSR values are reasonably accurate and comparable with the currently existing DSR product from GEWEX-SRB but at a higher spatial resolution although some discrepancies still exist in the model-computed DSR.

2) Evaluation and Comparison at a Monthly Time Scale: High-quality monthly mean DSR ground measurements data were collected from 525 stations in three networks, including 36 stations from BSRN, 94 stations from CDC/CMA, and 395 stations from GEBA. As mentioned earlier in this paper, the daily mean DSR was directly provided only by GEWEX-SRB among the selected data products. The latest satellite retrieval of the DSR provided by CERES-EBAF has been reported to show higher accuracy than other gridded DSR products [4], [5], [31], [56] because it uses more accurate cloud input data for calculating DSR. Zhang *et al.* [56] found that the ERA-Interim DSR showed a relatively higher

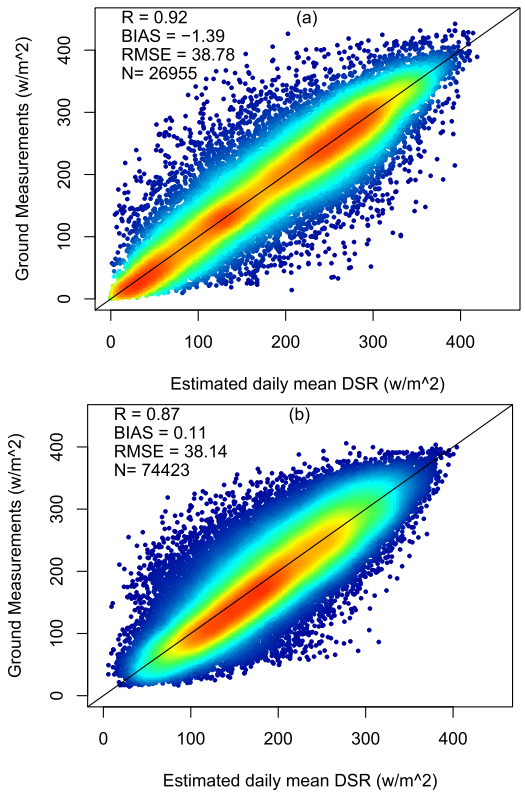

Fig. 7. As in Fig. 6, but for comparison between GEWEX-SRB and ground measurements from (a) BSRN and (b) CDC/CMA.

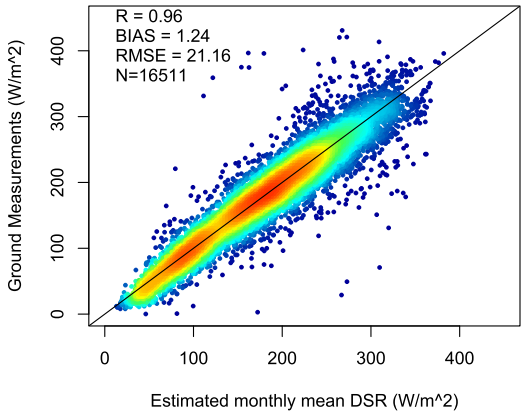

Fig. 8. Scatter plot comparison between the model computed and the ground measurements of monthly average DSR at 36 stations from BSRN, 94 stations from the CDC/CMA, and 395 stations from the GEBA, over the time period 2003–2005, respectively. R and N are the correlation coefficient and the number of matched data pairs, respectively.

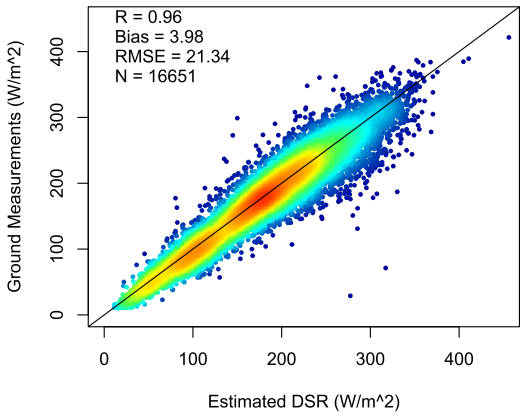

Fig. 9. As in Fig. 8, but for comparison between GEWEX-SRB and ground measurements.

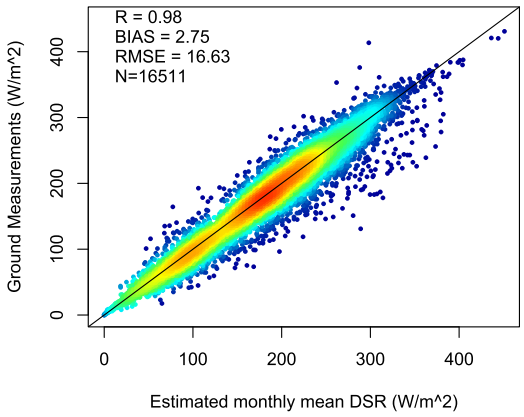

Fig. 10. As in Fig. 8, but for but for comparison between CERES-EBAF and ground measurements.

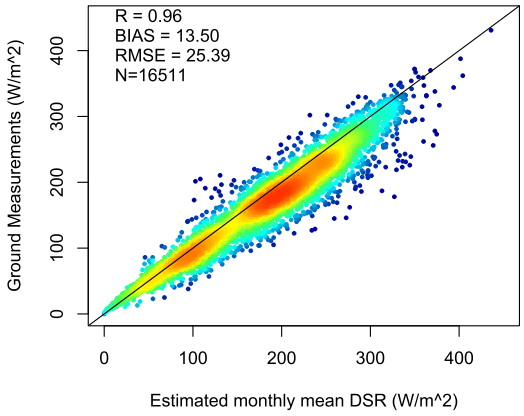

Fig. 11. As in Fig. 8, but for comparison between ERA-Interim and ground measurements.

precision by evaluating the DSR estimates from six global reanalyses using ground measurements collected from 674 stations. Therefore, these three existing radiation products were chosen for comparison.

Fig. 8 shows a scatterplot representing a comparison of the ground measurements versus the model-computed monthly mean DSR within $1^\circ \times 1^\circ$ cell containing each of the selected 525 stations. The model-computed DSR correlated very well with the corresponding DSR collected from the selected stations at a monthly time scale. The model-computed DSR had an overall R value of 0.96, a positive bias of 1.24 W/m^2, and an RMSE of 21.16 W/m^2. Evaluations were also conducted for GEWEX-SRB, CERES-EBAF, and ERA-Interim, as shown in Figs. 9–11, respectively. ERA-Interim exhibited the worst performance, compared to other DSR data at the selected stations, with an R value of 0.96, a positive bias value of 13.50 W/m^2, and an RMSE value of 25.39 W/m^2. CERES-EBAF had the highest R value and lowest RMSE, compared to those calculated for the other three DSR estimates, while the model-computed DSR had the lowest bias compared to the other three existing DSR products. Table IV shows

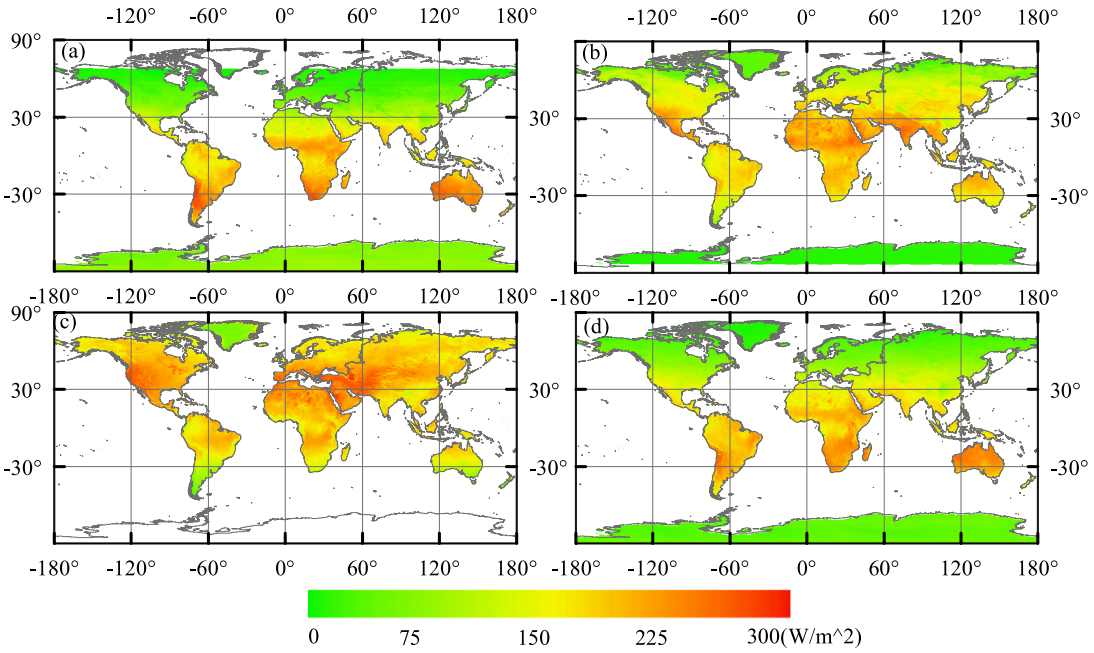

Fig. 12. Three-year (2003–2005) average global land distribution of SSNR (in W/m^2) at 5-km spatial resolution at the earth's surface for (a) winter (DJF), (b) spring (MAM), (c) summer (JJA), and (d) autumn (SON) seasons.

TABLE IV

EVALUATION OF THE MONTHLY DSR FROM MODEL COMPUTED, GEWEX-SRB, CERES-EBAF, AND ERA-INTERIM, THE SETS USING SURFACE MEASUREMENTS AT 36 STATIONS FROM BSRN, 94 STATIONS FROM THE CDC/CMA, AND 395 STATIONS FROM THE GEBA OVER THE TIME PERIOD 2003–2005. UNITS ARE W/M^2 FOR BIAS AND RMSE

Data sources	Measures	BSRN	GEBA	CMA	All networks
Model computed	R	0.97	0.97	0.93	0.96
	Bias	-6.39	0.38	9.63	1.24
	RMSE	22.87	17.67	24.41	21.16
GEWEX-SRB	R	0.97	0.96	0.95	0.96
	Bias	-1.92	4.10	5.48	3.98
	RMSE	21.21	21.41	21.12	21.34
CERES-EBAF	R	0.99	0.98	0.96	0.98
	Bias	-1.08	1.80	7.27	2.75
	RMSE	11.88	16.09	19.49	16.63
ERA-interim	R	0.99	0.97	0.93	0.96
	Bias	7.19	11.62	22.01	13.50
	RMSE	16.55	23.78	32.13	25.39

the validation results for the DSR monthly values of the model-computed DSR and the current three existing DSR products by comparison with the ground measurements at the 524 selected stations. Table IV also shows the statistical measures calculated using the various surface observation network sources as evaluation data. The model-computed monthly DSR product had an overall R of 0.97, a negative bias of −6.39, and an RMSE of 22.87 W/m^2 when the BSRN observations were used as validation data. When GEBA and CDC/CMA were used as validation data, the biases were 0.38 and 9.63 W/m^2, respectively. The GEWEX-SRB monthly DSR product had an overall R of 0.97, a negative bias of −1.92 W/m^2, and an RMSE of 21.21 W/m^2 when the BSRN observations were used as validation data. When GEBA and CDC/CMA were used as validation data, the biases were 4.10 and 5.48 W/m^2, respectively. When BSRN, GEBA, and CDC/CMA were used as validation data, the biases were −1.08, 1.80, and 7.27 W/m^2, respectively. ERA-Interim overestimated the DSR, compared to the selected surface observational networks. The biases were 7.19, 11.62, and 22.01 W/m^2 when BSRN, GEBA, and CDC/CMA were used as validation data, respectively. The validation results at a monthly scale further indicated that the model-computed DSR is reasonably accurate and comparable with the existing DSR product.

C. Spatial Distribution

Figs. 12 and 13 display the model-computed monthly SSNR and DSR climatologies for December, January, and February (DJF), March, April, and May (MAM), June, July, and August (JJA), and September, October, and December (SON), respectively. According to Figs. 12 and 13, the SSNRs at the earth's surface are similar to the DSR fluxes. The differences between the SSNR and DSR are quite small in most areas. The major differences between the SSNR and DSR are found over the brighter surfaces, such as deserts or snow- and ice-covered Polar Regions. In Fig. 13, the biases between the model-computed multiyear annual mean DSR product and the CERES-EBAF DSR product (GLASS minus CERES-EBAF) over the time period 2003–2005 are also shown. As shown in Fig. 13, the CERES-EBAF DSR climatology for DJF indicates that a greater DSR was received between the latitudinal bands of −30° S and 30° S and in the Antarctic in DJF, whereas smaller DSR values was received in the Northern Hemisphere. The latitudinal variation in the multiyear averaged DSR at the earth's surface is primarily determined by the incoming solar radiation at the TOA, while the longitudinal variation patterns are mostly determined by aerosol, cloud, and surface properties. Therefore, large values of DSR are found in the Polar Regions in winter and high-latitude areas in summer. It

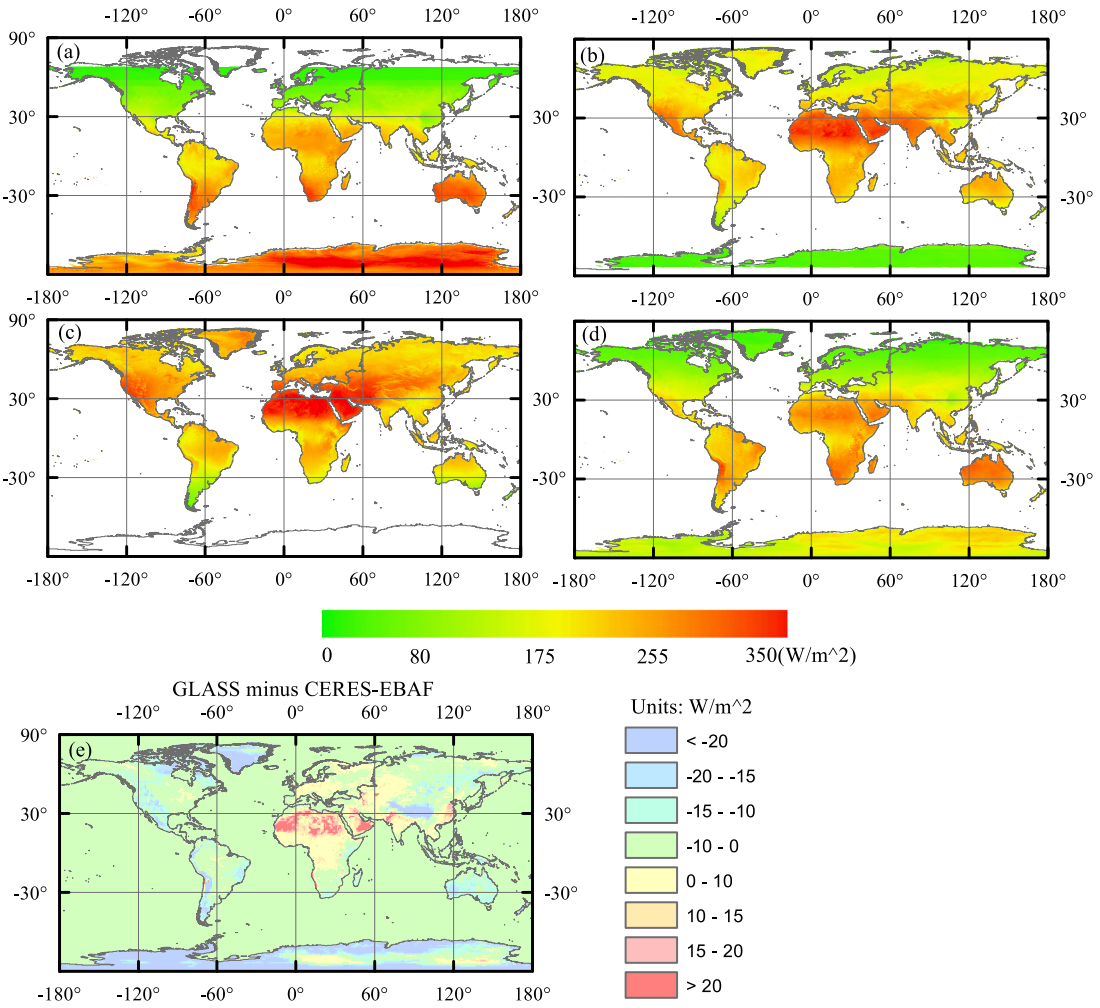

Fig. 13. Three-year (2003–2005) average global land distribution of DSR (in W/m^2) at 5-km spatial resolution at the earth's surface for (a) winter (DJF), (b) spring (MAM), (c) summer (JJA), and (d) autumn (SON) seasons, and (e) the biases between the model computed multiyear annual mean DSR product and the CERES-EBAF DSR product (GLASS minus CERES-EBAF).

is clear that there is a gradual DSR decrease from the summer to winter poles in winter and summer (see Fig. 13), leading to zero values poleward of mid-latitude to high latitude. The three-year (2003–2005) annual mean DSR differences between the model-computed annual mean DSR and the CERES-EBAF DSR product (GLASS minus CERES-EBAF) are shown in Fig. 13(e). The maximum differences from CERES-EBAF occurred at high latitudes, especially in the Antarctic and Greenland areas, where the solar zenith angle is large, and the surfaces are mainly covered with snow or ice, and as well as the brighter surfaces, such as North Africa. The model-computed DSR estimates are greater than the CERES-EBAF estimates in Southeastern China, whereas they are lower than the CERES-EBAF estimates over the Tibetan Plateau.

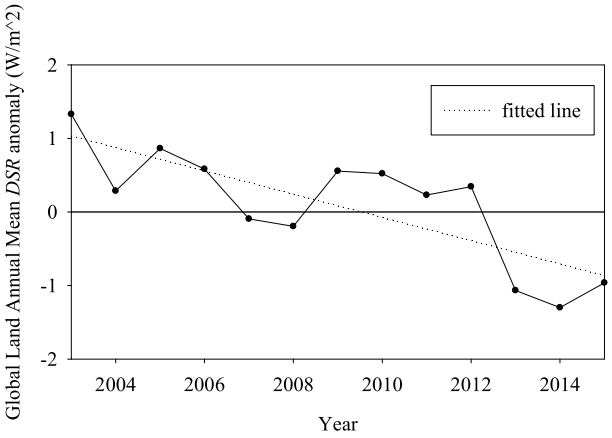

Fig. 14. Global land long-term variability of the model computed DSR.

D. Annual Mean and Long-Term Variability

Much effort has been reported to estimate the global annual mean DSR values from different data sources, including ground measurements, retrievals from satellite observations, reanalysis data, and simulation from global circulation models [31], [56], [57]. The annual mean DSR calculated from the 13-year model-computed DSR data was 184.8 W/m^2 over land, which was close to the latest reported value of 185 W/m^2 by Wild *et al.* [31]. However, the discrepancies between the DSR estimates and the ground measurements may introduce certain uncertainties into the annual mean DSR estimates. The long-term global annual variability in the model-computed DSR was also shown in this paper (see Fig. 14). The global model-computed DSR data showed a significant dimming

trend from 2003 to 2015, with a decreasing trend of 0.4 W/m^2/decade.

V. Conclusion

Knowledge of the radiation budget at earth's surface is essential for improving our understanding of earth's climate. Therefore, methods for estimating long-term DSR products at earth's surface are important for climate studies. Moreover, current methods for estimating DSR suffer from difficulties in quantifying clouds, aerosols, and the interactions between cloud and aerosol effects. Previous studies have shown that current existing DSR estimates, either from satellite observations or global reanalysis products, cannot reproduce long-term DSR variability very well and that clouds and aerosols used as inputs in their model determine the DSR variation trends [5], [56].

This paper attempted to estimate SSNR and DSR globally at a higher spatial resolution (i.e., 5 km) based on an operational scheme. Different from previous method for estimating SSNR and DSR using additional cloud and aerosol data as inputs, SSNR and DSR were estimated in this paper using satellite-observed TOA reflectances directly. The generated SSNR and DSR data were evaluated against ground measurements extensively collected from various ground observation networks. The developed SSNR data had an overall R value of 0.93 (0.96), a bias of 8.82 (9.87) W/m^2, and an RMSE of 28.22 (32.84) W/m^2 at the BSRN and CDC/CMA stations at a daily (monthly) time scale, while the DSR estimates had an R value of 0.92 (0.96), a bias of 3.72 (1.24) W/m^2, and an RMSE of 32.84 (21.16) W/m^2 at the BSRN and CDC/CMA stations at a daily (monthly) time scale. The validation results indicated that the model-computed SSNR and DSR data are reasonably consistent with those measured of ground-level but with a higher spatial resolution (5 km) than the existing products ($\sim$100 km).

Although the validation results showed that the model-computed SSNR and DSR correlated well with the corresponding ground measurements, some outlier points were found in the validation scatter plots. As discussed in Section IV, a detailed analysis of the validation results for the SSNR and DSR against the ground measurements from the BSRN stations shows that the large biases were found at two high-latitude stations for both SSNR and DSR. This is mainly due to the underestimation of GLASS albedo in high latitude, especially over the snow- and ice-covered Polar Regions (Qiang Liu and Yin Qu, personal communication in 2017). Different biases between SSNR and DSR may come from different numbers of ground measurements of SSNR and DSR employed in the evaluation. Currently, about 20 and 500 *in situ* measurements of SSNR and DSR, respectively, are available for the purpose. Besides, different measurement errors of SSNR and DSR (e.g., instrument sensitivity technical failures and instrument replacement) may also cause different biases in the SSNR and DSR evaluation. Furthermore, scaling issues and urbanization effect could also be potential error sources for SSNR and DSR evaluation. Thus, more effort should be put to fully understand the bias differences between estimated SSNR and DSR.

It was also found that the model-computed DSR and the three selected DSR products from satellite observations and global reanalysis are overestimated at the CDC/CMA stations compared to the direct ground measurements. The mean biases of the monthly mean DSR were 9.63, 5.48, 7.27, and 22.01 W/m^2 for the model-computed, GEWEX-SRB, CERES-EBAF, and ERA-Interim data, respectively. There are many factors that may cause potential uncertainties in the DSR estimation. First, the developed retrieval method may have some limitations. For example, cloud and aerosol are two important factors to regulate the DSR. Therefore, the cloud and aerosol schemes presented in the retrieval model may cause errors in the DSR estimates. In addition, although the regression coefficients for the proposed method in this paper were obtained from an extensive atmospheric radiative transfer simulation using MODTRAN under representative surface and atmospheric conditions, MODTRAN has some issues for radiative transfer simulating under larger solar zenith angle conditions as a plane-parallel radiative transfer model [55]. Besides, the measurement errors, scaling issues, and urbanization effects may also be other potential error sources.

Although the generated SSNR and DSR correlate well with the corresponding ground-measured values at most stations selected in this paper, some discrepancies still exist in the SSNR and DSR estimates. Much work and efforts are still required for surface radiation and energy budget studies; these include collecting high-quality ground measurements, improving DSR estimates from satellite observations, and refining cloud and aerosol schemes in physical models.

References

[1] H. M. Deneke, A. J. Feijt, and R. A. Roebeling, "Estimating surface solar irradiance from METEOSAT SEVIRI-derived cloud properties," *Remote Sens. Environ.*, vol. 112, no. 6, pp. 3131–3141, Jun. 2008.

[2] N. Hatzianastassiou and I. Vardavas, "Shortwave radiation budget of the northern hemisphere using International Satellite Cloud Climatology Project and NCEP/NCAR climatological data," *J. Geophys. Res., Atmos.*, vol. 104, no. D20, pp. 24401–24421, 1999.

[3] Z. Li, H. O. Leighton, and R. D. Cess, "Surface net solar radiation estimated from satellite measurements: Comparisons with tower observations," *J. Climate*, vol. 6, no. 9, pp. 1764–1772, 1993.

[4] M. Wild, D. Folini, C. Schär, N. Loeb, E. G. Dutton, and G. König-Langlo, "The global energy balance from a surface perspective," *Climate Dyn.*, vol. 40, nos. 11–12, pp. 3107–3134, 2012.

[5] X. Zhang, S. Liang, M. Wild, and B. Jiang, "Analysis of surface incident shortwave radiation from four satellite products," *Remote Sens. Environ.*, vol. 165, pp. 186–202, Aug. 2015.

[6] T. He, S. Liang, D. Wang, Q. Shi, and M. L. Goulden, "Estimation of high-resolution land surface net shortwave radiation from AVIRIS data: Algorithm development and preliminary results," *Remote Sens. Environ.*, vol. 167, pp. 20–30, Sep. 2015.

[7] H.-Y. Kim and S. Liang, "Development of a hybrid method for estimating land surface shortwave net radiation from MODIS data," *Remote Sens. Environ.*, vol. 114, no. 11, pp. 2393–2402, 2010.

[8] D. Wang, S. Liang, T. He, and Q. Shi, "Estimation of daily surface shortwave net radiation from the combined MODIS data," *IEEE Trans. Geosci. Remote Sens.*, vol. 53, no. 10, pp. 5519–5529, Oct. 2015.

[9] N. Hatzianastassiou *et al.*, "Global distribution of Earth's surface shortwave radiation budget," *Atmos. Chem. Phys. Discussions*, vol. 5, no. 10, pp. 2847–2867, 2005.

[10] S. Liang, T. Zheng, R. Liu, H. Fang, S. C. Tsay, and S. Running, "estimation of incident photosynthetically active radiation from moderate resolution imaging spectrometer data," (in English), *J. Geophys. Res.-Atmos., Article*, vol. 111, no. D15, p. D15208, Aug. 2006.

[11] N. Lu, R. Liu, J. Liu, and S. Liang, "An algorithm for estimating downward shortwave radiation from GMS 5 visible imagery and its evaluation over China," *J. Geophys. Res., Atmos.*, vol. 115, no. D18, p. D18102, 2010.

[12] Y. Ma and R. T. Pinker, "Modeling shortwave radiative fluxes from satellites," *J. Geophys. Res., Atmos.*, vol. 117, no. D23, p. D23202, 2012.

[13] R. W. Mueller, C. Matsoukas, A. Gratzki, H. D. Behr, and R. Hollmann, "The CM-SAF operational scheme for the satellite based retrieval of solar surface irradiance—A LUT based eigenvector hybrid approach," *Remote Sens. Environ.*, vol. 113, no. 5, pp. 1012–1024, 2009.

[14] R. T. Pinker and I. Laszlo, "Modeling surface solar irradiance for satellite applications on a global scale," *J. Appl. Meteorol.*, vol. 31, no. 2, pp. 194–211, 1992.

[15] R. T. Pinker *et al.*, "Surface radiation budgets in support of the GEWEX Continental-Scale International Project (GCIP) and the GEWEX Americas Prediction Project (GAPP), including the North American Land Data Assimilation System (NLDAS) project," *J. Geophys. Res., Atmos.*, vol. 108, no. D22, p. 8844, 2003.

[16] R. Posselt, R. W. Mueller, R. Stöckli, and J. Trentmann, "Remote sensing of solar surface radiation for climate monitoring—The CM-SAF retrieval in international comparison," *Remote Sens. Environ.*, vol. 118, pp. 186–198, Mar. 2012.

[17] Y. Ryu, S. Kang, S.-K. Moon, and J. Kim, "Evaluation of land surface radiation balance derived from moderate resolution imaging spectroradiometer (MODIS) over complex terrain and heterogeneous landscape on clear sky days," *Agricult. Forest Meteorol.*, vol. 148, pp. 1538–1552, Sep. 2008.

[18] H. Wang and R. T. Pinker, "Shortwave radiative fluxes from MODIS: Model development and implementation," *J. Geophys. Res.*, vol. 114, no. D20, p. D20201, 2009.

[19] X. Zhang, S. Liang, G. Zhou, H. Wu, and X. Zhao, "Generating Global Land Surface Satellite incident shortwave radiation and photosynthetically active radiation products from multiple satellite data," *Remote Sens. Environ.*, vol. 152, pp. 318–332, Sep. 2014.

[20] Y. C. Zhang, W. B. Rossow, and A. A. Lacis, "Calculation of surface and top of atmosphere radiative fluxes from physical quantities based on ISCCP data sets: 1. Method and sensitivity to input data uncertainties," *J. Geophys. Res., Atmos.*, vol. 100, no. D1, pp. 1149–1165, 1995.

[21] Y. L. Zhang, B. Q. Qin, and W. M. Chen, "Analysis of 40 year records of solar radiation data in Shanghai, Nanjing and Hangzhou in Eastern China," *Theor. Appl. Climatol., J. Article*, vol. 78, no. 4, pp. 217–227, Aug. 2004.

[22] J. Qin, W. Tang, K. Yang, N. Lu, X. Niu, and S. Liang, "An efficient physically based parameterization to derive surface solar irradiance based on satellite atmospheric products," *J. Geophys. Res., Atmos.*, vol. 120, no. 10, p. 2015JD023097, 2015.

[23] W. Tang, K. Yang, Z. Sun, J. Qin, and X. Niu, "Global performance of a fast parameterization scheme for estimating surface solar radiation from MODIS data," *IEEE Trans. Geosci. Remote Sens.*, vol. 55, no. 6, pp. 3558–3571, Jun. 2017.

[24] W. Tang, J. Qin, K. Yang, S. Liu, N. Lu, and X. Niu, "Retrieving high-resolution surface solar radiation with cloud parameters derived by combining MODIS and MTSAT data," (in English), *Atmos. Chem. Phys., Article*, vol. 16, no. 4, pp. 2543–2557, 2016.

[25] G. Bisht, V. Venturini, S. Islam, and L. Jiang, "Estimation of the net radiation using MODIS (Moderate Resolution Imaging Spectroradiometer) data for clear sky days," *Remote Sens. Environ.*, vol. 97, no. 1, pp. 52–67, Jul. 2005.

[26] G. Huang, S. Liu, and S. Liang, "Estimation of net surface shortwave radiation from MODIS data," *Int. J. Remote Sens.*, vol. 33, no. 3, pp. 804–825, 2012.

[27] Z. Li, H. G. Leighton, K. Masuda, and T. Takashima, "Estimation of SW flux absorbed at the surface from TOA reflected flux," *J. Climate*, vol. 6, no. 2, pp. 317–330, 1993.

[28] B. Tang, Z.-L. Li, and R. Zhang, "A direct method for estimating net surface shortwave radiation from MODIS data," *Remote Sens. Environ.*, vol. 103, pp. 115–126, Jul. 2006.

[29] S. Gui, S. Liang, K. Wang, L. Li, and X. Zhang, "Assessment of three satellite-estimated land surface downwelling shortwave irradiance data sets," *IEEE Geosci. Remote Sens. Lett.*, vol. 77, no. 4, pp. 776–780, Oct. 2010.

[30] S. Liang, K. Wang, X. Zhang, and M. Wild, "Review on estimation of land surface radiation and energy budgets from ground measurement, remote sensing and model simulations," *IEEE J. Sel. Topics Appl. Earth Observ. Remote Sens.*, vol. 3, no. 3, pp. 225–240, Sep. 2010.

[31] M. Wild *et al.*, "The energy balance over land and oceans: An assessment based on direct observations and CMIP5 climate models," (in English), *Climate Dyn.*, vol. 44, nos. 11–12, pp. 3393–3429, 2015.

[32] R. Urraca *et al.*, "Extensive validation of CM SAF surface radiation products over Europe," *Remote Sens. Environ.*, vol. 199, pp. 171–186, Sep. 2017.

[33] Q. Liu *et al.*, "Preliminary evaluation of the long-term GLASS albedo product," *Int. J. Digit. Earth*, vol. 6, pp. 69–95, Dec. 2013.

[34] J. Qin *et al.*, "Evaluation of surface albedo from GEWEX-SRB and ISCCP-FD data against validated MODIS product over the Tibetan Plateau," *J. Geophys. Res., Atmos.*, vol. 116, no. D24, p. D24116, 2011.

[35] K. Wang, S. Liang, C. L. Schaaf, and A. H. Strahler, "Evaluation of moderate resolution imaging spectroradiometer land surface visible and shortwave albedo products at FLUXNET sites," *J. Geophys. Res., Atmos.*, vol. 115, no. D17, p. D17107, 2010.

[36] R. D. Cess, E. G. Dutton, J. J. Deluisi, and F. Jiang, "Determining surface solar absorption from broadband satellite measurements for clear skies: Comparison with surface measurements," *J. Climate*, vol. 4, no. 2, pp. 236–247, 1991.

[37] R. D. Cess and I. L. Vulis, "Inferring surface solar absorption from broadband satellite measurements," *J. Climate*, vol. 2, no. 9, pp. 974–985, 1989.

[38] B. Jia, Z. Xie, A. Dai, C. Shi, and F. Chen, "Evaluation of satellite and reanalysis products of downward surface solar radiation over East Asia: Spatial and seasonal variations," *J. Geophys. Res., Atmos.*, vol. 118, pp. 3431–3446, 2013.

[39] R. Posselt, R. Mueller, J. Trentmann, R. Stockli, and M. A. Liniger, "A surface radiation climatology across two Meteosat satellite generations," *Remote Sens. Environ.*, vol. 142, pp. 103–110, Feb. 2014.

[40] Y. Zhang, W. B. Rossow, A. A. Lacis, V. Oinas, and M. I. Mishchenko, "Calculation of radiative fluxes from the surface to top of atmosphere based on ISCCP and other global data sets: Refinements of the radiative transfer model and the input data," *J. Geophys. Res., Atmos.*, vol. 109, no. D19, p. D19105, 2004.

[41] S. Kato *et al.*, "Surface irradiances consistent with CERES-derived top-of-atmosphere shortwave and longwave irradiances," *J. Climate*, vol. 26, no. 9, pp. 2719–2740, 2013.

[42] S. Kato *et al.*, "Improvements of top-of-atmosphere and surface irradiance computations with CALIPSO-, CloudSat-, and MODIS-derived cloud and aerosol properties," *J. Geophys. Res., Atmos.*, vol. 116, no. D19. p. D19209, 2011.

[43] W. Tang, J. Qin, K. Yang, X. Niu, M. Min, and S. Liang, "An efficient algorithm for calculating photosynthetically active radiation with MODIS products," *Remote Sens. Environ.*, vol. 194, pp. 146–154, Jun. 2017.

[44] K. Yang *et al.*, "Evaluation of satellite estimates of downward shortwave radiation over the Tibetan Plateau," *J. Geophys. Res., Atmos.*, vol. 113, no. D17, p. D17204, 2008.

[45] H. Gilgen and A. Ohmura, "The global energy balance archive," *Bull. Amer. Meteorol. Soc.*, vol. 80, no. 5, pp. 831–850, 1999.

[46] *Members-of-the-MODIS-Characterization-Support-Team, MODIS Level 1B Product User's Guide*, NASA/Goddard Space Flight Center, Greenbelt, MD, USA, 2012, p. 57.

[47] M. Nishihama *et al.*, "MODIS level 1A Earth locations: Algorithm theoretical basis document Version 3.0," NASA/Goddard Space Flight Center, Greenbelt, MD, USA, Tech. Rep., 1997.

[48] S. Ackerman, K. Strabala, P. Menzel, R. Frey, C. Moeller, and L. Gumley, "Discriminating clear-sky from cloud with MODIS algorithm theoretical basis document (MOD35)," MODIS Cloud Mask Team, Cooperat. Inst. Meteorol. Satell. Stud., Univ. Wisconsin, Madison, WI, USA, 2010.

[49] Y. Qu, Q. Liu, S. Liang, L. Wang, N. Liu, and S. Liu, "Direct-estimation algorithm for mapping daily land-surface broadband albedo from MODIS data," *IEEE Trans. Geosci. Remote Sens.*, vol. 52, no. 2, pp. 907–919, Feb. 2014.

[50] A. Simmons, S. Uppala, D. Dee, and S. Kobayashi, "ERAInterim: New ECMWF reanalysis products from 1989 onwards," ECMWF Newsletter, Reading, U.K., Appl. Note 110, 2006, pp. 25–35.

[51] D. P. Dee *et al.*, "The ERA-Interim reanalysis: Configuration and performance of the data assimilation system," *Quart. J. Roy. Meteorol. Soc.*, vol. 137, pp. 553–597, Apr. 2011.

[52] E. J. Mlawer, S. J. Taubman, P. D. Brown, M. J. Iacono, and S. A. Clough, "Radiative transfer for inhomogeneous atmospheres: RRTM, a validated correlated-k model for the longwave," *J. Geophys. Res.*, vol. 102, no. D14, pp. 16663–16682, 1997.

[53] M. Wild, "Enlightening global dimming and brightening," *Bull. Amer. Meteorol. Soc.*, vol. 93, no. 1, pp. 27–37, Jan. 2012.
[54] V. Ramanathan, P. J. Crutzen, J. T. Kiehl, and D. Rosenfeld, "Aerosols, climate, and the hydrological cycle," *Science*, vol. 294, no. 5549, pp. 2119–2124, 2001.
[55] N. G. Loeb and R. Davies, "Observational evidence of plane parallel model biases: Apparent dependence of cloud optical depth on solar zenith angle," *J. Geophys. Res., Atmos.*, vol. 101, no. D1, pp. 1621–1634, 1996.
[56] X. Zhang, S. Liang, G. Wang, Y. Yao, B. Jiang, and J. Cheng, "Evaluation of the reanalysis surface incident shortwave radiation products from NCEP, ECMWF, GSFC, and JMA using satellite and surface observations," *Remote Sens.*, vol. 8, no. 3, p. 225, 2016.
[57] Q. Ma, K. C. Wang, and M. Wild, "Impact of geolocations of validation data on the evaluation of surface incident shortwave radiation from Earth System Models," *J. Geophys. Res., Atmos.*, vol. 120, no. 14, pp. 6825–6844, Jul. 2015.

Xiaotong Zhang received the Ph.D. degree in cartography and geographic information science from Wuhan University, Wuhan, China, in 2010.

He was a joint Ph.D. Student with the Department of Geographical Sciences, University of Maryland at College Park, College Park, MD, USA. He is currently a Visiting Scholar with the Nicholas School of the Environment, Duke University, Durham, NC, USA, and also an Associate Professor with the State Key Laboratory of Remote Sensing Science, jointly sponsored by Beijing Normal University and the Institute of Remote Sensing and Digital Earth, Chinese Academy of Sciences, Faculty of Geographical Science, Beijing Normal University, Beijing, China. His research interests include the estimation of land surface radiation parameters using satellite data and the studies on global energy budget.

Dongdong Wang received the B.S. degree in environmental sciences from Peking University, Beijing, China, and the Ph.D. degree in geography from the University of Maryland at College Park, College Park, MD, USA.

He is currently an Associate Research Professor with the Department of Geographical Sciences, University of Maryland at College Park. His research interests include remote sensing of surface radiation budget, integration of high-level remote sensing land products, climate change, and terrestrial ecosystem.

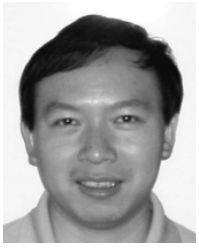

Qiang Liu received the B.S. degree in computational mathematics from Beijing University, Beijing, China, in 1997, and the Ph.D. degree in cartography and remote sensing from the Institute of Remote Sensing Applications, Chinese Academy of Sciences (CAS), Beijing, in 2002.

He is currently an Associate Professor with the College of Global Change and Earth System Science, Beijing Normal University, Beijing, and the State Key Laboratory of Remote Sensing Science, jointly sponsored by the Institute of Remote Sensing and Digital Earth, CAS, and Beijing Normal University. His research interests include multiangular remote sensing, BRDF/albedo modeling, component temperature retrieval, generating long time series of global BRDF/albedo from multiple remote sensing data sources, and snow/seaice albedo variation in polar regions.

Yunjun Yao received the Ph.D. degree from Peking University, Beijing, China, in 2010.

From 2008 to 2009, he was a joint Ph.D. Student with the Department of Geographical Sciences, University of Maryland at College Park, College Park, MD, USA. He is currently with the State Key Laboratory of Remote Sensing Science, Faculty of Geographical Science, Beijing Normal University, Beijing. His research interests include the estimation of evapotranspiration and the retrieval of surface biophysical parameters by remote sensing.

Kun Jia received the B.S. degree in surveying and mapping engineering from Central South University, Changsha, China, in 2006, and the Ph.D. degree in cartography and geographical information system from Institute of Remote Sensing Applications, Chinese Academy of Sciences, Beijing, China in 2011.

He is currently an Associate Professor with the State Key Laboratory of Remote Sensing Science and the Beijing Engineering Research Center for Global Land Remote Sensing Products, Faculty of Geographical Science, Beijing Normal University, Beijing. His research interests include the estimation of vegetation parameters, land cover classification, and agriculture monitoring using remote sensing data.

Tao He received the B.E. degree in photogrammetry and remote sensing from Wuhan University, Wuhan, China, in 2006, and the Ph.D. degree in geography from the University of Maryland at College Park, College Park, MD, USA, in 2012.

He was an Assistant Research Professor with the Department of Geographical Sciences, University of Maryland at College Park. He is currently a Professor with the School of Remote Sensing and Information Engineering, Wuhan University. His research interests include surface anisotropy and albedo modeling, data fusion of satellite products, and long-term regional and global surface radiation budget analysis.

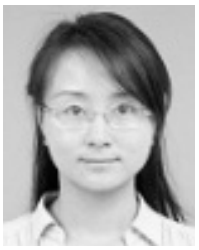

Bo Jiang received the B.S. degree in mapping and surveying engineer from Central South University, Changsha, China, in 2006, and the M.E. degree in cartography and geographical information system and the Ph.D. degree from Beijing Normal University, Beijing, China, in 2009 and 2012, respectively.

From 2010 to 2012, she was a joint Ph.D. Student with the Department of Geographical Sciences, University of Maryland at College Park, College Park, MD, USA. She is currently with the Faculty of Geographical Science, Institute of Remote Sensing Science and Engineering, Beijing Normal University. Her research interests include net radiation estimation by using remote sensing data, time series analysis, assessing the impacts of the land cover change on the climate from various observations, and application of remote sensing products.

Yu Wei is currently pursuing the M.S. degree in cartography and geographical information system with the State Key Laboratory of Remote Sensing Science, Faculty of Geographical Science, Beijing Normal University, Beijing, China.

Her research interests include the estimation of land surface radiation components from satellite data.

Han Ma received the B.S. degree from the Shandong University of Science and Technology, Qingdao, China, in 2010, and the M.S. and Ph.D. degrees from Beijing Normal University, Beijing, China, in 2013 and 2018, respectively.

In 2017, she was a joint Ph.D. Student with the Department of Geographical Sciences, University of Maryland at College Park, College Park, MD, USA. She is currently continuing her Post-Doctoral Research at Wuhan University, Wuhan, China. Her research interests include radiative transfer model and inversion of land and atmosphere surface parameters.

Xiang Zhao received the Ph.D. degree in cartography and geographic information system from the School of Geography, Beijing Normal University, Beijing, China, in 2006.

From 2008 to 2010, he was a Post-Doctoral Fellow with the College of Resources Science and Technology, Beijing Normal University. He is currently with the State Key Laboratory of Remote Sensing Science, jointly sponsored by Beijing Normal University and the Institute of Remote Sensing and Digital Earth, Chinese Academy of Sciences, Faculty of Geographical Science, Beijing Normal University. His research interests include high-performance computing system construction and quantitative remote sensing application. He also did some research about long time series remote sensing data trend analysis.

Wenhong Li received the Ph.D. degree from the Georgia Institute of Technology, Atlanta, GA, USA.

She is currently an Associate Professor with the Division of Earth and Ocean Sciences, Nicholas School of the Environment, Duke University, Durham, NC, USA. Her research interests include climate dynamics, land–atmosphere interaction, hydroclimatology, climate modeling, and to understand how the hydrological cycle changes in the current and future climate and their impacts on the ecosystems, subtropical high variability and change, unforced global temperature variability, and climate and health issues.

Dr. Li is an Editor of the *Journal of Climate*.

Shunlin Liang (M'94–F'13) received the Ph.D. degree from Boston University, Boston, MA, USA.

He is currently a Professor with the Department of Geographical Sciences, University of Maryland at College Park, College Park, MD, USA, and the State Key Laboratory of Remote Sensing Science, School of Geography, Beijing Normal University, Beijing, China. He has published over 220 peer-reviewed journal papers, authored the book *Quantitative Remote Sensing of Land Surfaces* (Wiley, 2004), coauthored the book *Global LAnd Surface Satellite (GLASS) Products: Algorithms, Validation and Analysis* (Springer, 2013), edited the book *Advances in Land Remote Sensing: System, Modeling, Inversion and Application* (Springer, 2008), and coedited the books *Advanced Remote Sensing: Terrestrial Information Extraction and Applications* (Academic Press, 2012) and *Land Surface Observation, Modeling, Data Assimilation* (World Scientific, 2013). His research interests include the estimation of land surface variables from satellite data, earth's energy balance, and assessment of environmental impacts of vegetation changes.

Dr. Liang was an Associate Editor of the IEEE TRANSACTIONS ON GEOSCIENCE AND REMOTE SENSING and a guest editor of several remote sensing-related journals.